Prototype Disaster Response Robot with Variable Size and Rigidity

Kodai Ochi and Mitsuharu Matsumoto *

Department of Informatics, The University of Electro-Communications, Chofu, Japan
Email: o2340004@edu.cc.uec.ac.jp (K.O.); mitsuharu.matsumoto@ieee.org (M.M.)
*Corresponding author

***Abstract*—Disaster response robots are designed to replace human workers in hazardous environments. When transporting such robots, transportation by aircraft is sometimes desirable because land routes are not always safe. The performance of disaster response robots is constantly improving; however, their volume and mass tend to increase, which makes current disaster response robots unsuitable for air transportation. Thus, robots with variable size and rigidity should be developed to facilitate effective and efficient air transport. Therefore, we developed a lightweight robot that can be stored in a small space. The prototype robot is composed of a lightweight sponge that can be vacuum compressed to save space during transportation and can be deployed from the air. After being transported to the site, the robot can return to its original size by opening the package and releasing it from compression. In addition, the robot's rigidity is realized using UV-curing resin. The robot is also equipped with a vibration propulsion mechanism, and we confirmed that the robot can move using this mechanism. Furthermore, the robot was found to be able to change direction and carry lightweight objects.**

***Keywords*—size change, stiffness change, soft robotics, disaster response robot**

I. Introduction

Recently, studies have reported on disaster response robots to solve problems in various environments that cannot be accessed by humans [1]. Robots equipped with crawlers have been designed to work in disaster environments on the ground [2–5]. In addition, multi-legged robots that move in three dimensions have been investigated [6–8], and snake-like robots that mimic the shape and locomotive abilities of snakes have been developed for use in closed spaces [9–11]. Some studies have also proposed robots that combine the above features [12]. However, as rescue robots become increasingly sophisticated, their structures tend to become more complex, larger, and heavier. When disaster response robots are deployed in disaster environments, it is frequently difficult to select an effective land route; thus, it is important to develop robots that can be transported by air. Our goal is to develop soft and lightweight disaster response robots that can be deployed from an aircraft.

In the robotics field, small robots have been studied actively [13–16]. For example, a starfish-inspired milli-soft robot has been developed previously [17]. Such small robots can easily enter narrow spaces; however, they are too small for use as disaster robots.

Thus, we investigate the feasibility of a robot that is both small and soft during transportation but can become sufficiently large and hard during operation.

Previous studies have investigated inflatable robots that can their increase volume by increasing air pressure. Inflatable robots have been designed with various shapes, including human-like robots [18, 19], arm-shaped robots [20–22], and sheet-shaped robots [23, 24]. However, inflatable robots are made of soft vinyl sheets, and their rigidity does not change. Thus, inflatable robots are not suitable for various tasks, e.g., transporting supplies needed by disaster response robots in the field.

To solve the problems, we focus on two materials, i.e., sponges, which are compressible foam materials, and Ultraviolet light curing resin (UV-curing resin), which can be cured by sunlight. Sponges are soft and light, and they can be deployed safely from the air. In addition, sponges are porous; thus, their volume can be reduced via vacuum compression when transported by air. If the compressed robot body is opened at a disaster site, the sponge will return to its original size; thus, much larger robots can be used at disaster sites. Sponges are porous; therefore, they can store large volumes of liquid. Consequently, we considered a method to increase the robot's rigidity by curing it with UV-curing resin. In this study, we developed a prototype and achieved locomotion using a vibration motor and attaching ratchet materials to the bottom of the robot. Evaluations confirmed that such robots can transport hex nuts.

II. Basic Concept

Fig. 1 shows a schematic diagram of the basic concept of the proposed robot. In the event of a severe disaster, major roads can be cut off, which makes it difficult to transport supplies and secure personnel to search for

Manuscript received January 6, 2024; revised February 15, 2024; accepted March 18, 2024; published June 6, 2024.

missing people. Disaster response robots are a promising approach to solving this problem.

However, many disaster response robots are made of hard metal; thus, each robot must be transported directly to the disaster area. To solve this problem, we investigate soft disaster response robots that can be deployed from the air. As shown in Fig. 1, the robot is miniaturized to reduce the storage space required when mounted on an aircraft. Once the soft robot arrives at the disaster site, it is enlarged to a size that is suitable for on-site work. In addition, the robot is hardened to improve its ability to perform work.

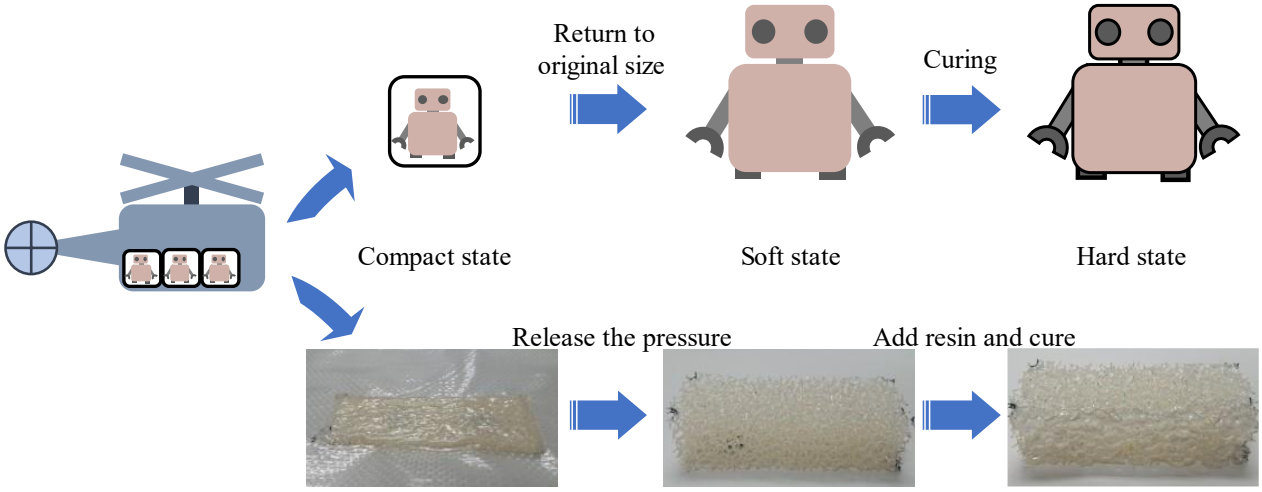

Fig. 1. Basic concept of the proposed robot. The top diagram shows the assumed scenario. The photographs show the sponges in each state.

In this study, we used sponges to enable the robot to change its size. To harden the robot during use, we utilized UV-curing resin, which can be cured by sunlight. During transportation, the soft sponge body of the robot is compressed by vacuum packing. After transportation, the robot is enlarged to its original size by releasing the pressure. We achieve greater hardness than the original sponge by curing the UV-curable resin that has penetrated into the sponge. The sponge is cut out according to its intended use before vacuum packing. Thus, the finished product can be prepared with simple operations at the disaster site. This approach reduces storage space during transportation. After expanding to the original size, the voids in the foam material can be filled with UV-curing resin to realize high hardness. As a simple implementation example, the prototype robot developed in this study employs vibration propulsion, which takes advantage of the characteristics of the robot's constituent sponge using vibration motors and ratchet materials.

III. Compact Strage of the Robot Body

Here, we describe the actual implementation method according to the flow of the scenario (Fig. 1). We also describe the compression of urethane, which is the constituent material of the robot. We envision that this compression will be performed in advance for air transport. The urethane sponges can be compressed from the outside to reduce their volume significantly, and they can return to their original size when the air pressure is released. Thus, we sealed the urethane foam sponge in a nylon-polyethylene sheet bag with a vacuum inside and compared the original and compressed sizes. Here, we used the VPF-385T (Iris Ohyama Inc.) vacuum-preserving food sealer to compress the urethane foam sponges. Its degassing power is approximately 66.7 kPa. This allows the air pressure inside the nylon-polyethylene sheet bag to be reduced to one-third of atmospheric pressure.

First, we cut out a 2 cm × 7 cm × 3 cm rectangle piece of urethane foam sponge. Then, a nylon-polyethylene sheet bag was prepared for vacuum packing. The nylon-polyethylene sheet bag was made of two nylon-polyethylene sheets. Its size was approximately 16 cm × 14 cm. The thickness of the bag was 0.35 mm. In addition, the urethane foam sponge was placed near the center of the nylon-polyethylene sheet bag with the 7 cm × 3 cm side facing the sheets. We then degassed the bag with the sponge inside and sealed it. Fig. 2 shows the deformation of the urethane foam sponge by vacuum compression. The flat size of the urethane foam sponge was generally unchanged before and after vacuum compression. However, the thickness of the sponge was compressed from approximately 2 cm to 3 mm, representing a 85% reduction in volume.

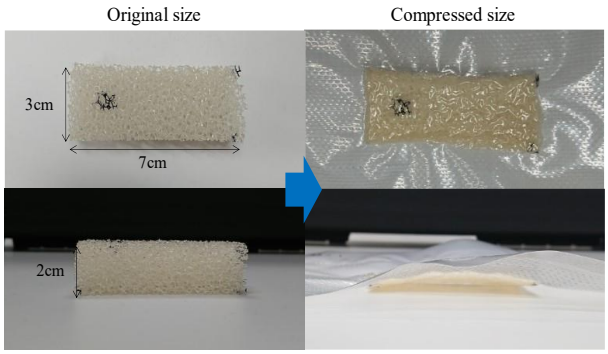

Fig. 2. Image of urethane foam sponge miniaturized by vacuum compression. The shrinkage is mainly noticeable in the vertical direction.

IV. Mechanical Propreties

A. Experimental Procedure

In our experimental scenario, we assumed that, after being deployed from the air, the robot should become large and rigid during the usage stage. Here, a three-point bending test was performed to investigate the stiffness of the urethane foam sponge cured via UV-curing resin. A urethane foam sponge with high porosity was used to facilitate the UV-curing resin process. Note that it is difficult to cut a sponge with high porosity; thus, the size of the test samples was relatively large, with approximate dimensions of 10 mm in thickness, 70 mm in length, and 20 mm in width. After cutting the sponge, we soaked it thoroughly in UV curing resin, placed it on a polyethylene sheet, and exposed it to UV light. Preparation of the sample was completed when the UV-curing resin was cured sufficiently. Using this process, a total of 14 samples were fabricated while varying the mass of the UV-curing resin in the sponge.

An MCT-2150 (A&D Co., Ltd.) force tester was attached to a jig to perform a three-point bending test. The radii of the upper and lower fulcrums of this jig were 5 mm, the rate of compression was 10 mm/min, and the distance between the fulcrums was 50 mm.

In this test, each sample was placed on the fulcrum stand with the surface faced it that was the bottom surface when the resin cured. The position of each sample was adjusted such that the force was applied near the center during the test.

B. Experimental Results

The urethane foam sponges were cut prior to conducting the experiments. The mass was approximately 0.4 g. These were filled with 0–8.8 g of UV-curing resin and cured. The mass of the UV-curing resin cured to the same size (70 mm × 20 mm ×10 mm) was approximately 13 g.

In the above samples, the three-point bending test was conducted. From this experiment, the deflection-bend load curves were obtained for each sample. In addition, the bending stresses were calculated from these curves. The bending stress value is calculated as follows:

$$\sigma = \frac{3F_{max}L}{2bh^2} \quad (1)$$

where σ and F_{max} are the bending stress and the maximum point of the bending load, respectively, and L, b, and h represent the distance between the fulcrums, the width of the test sample, and the thickness of the test sample, respectively. The bending stress value for the sample size was measured at five points at each distance prior to the test, and the average value was calculated for each sample.

Fig. 3 plots the relationship between the bending stress of each sample and the mass of the UV-curing resin in the sample. As can be seen, the bending stress increased as the mass of the UV-curing resin increased.

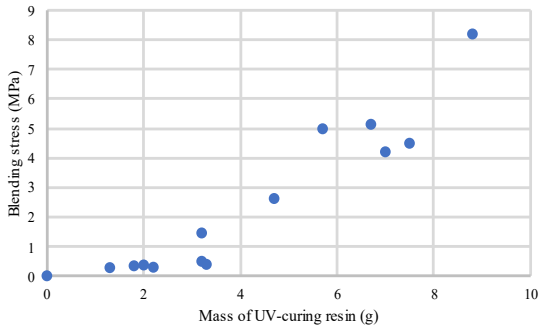

Fig. 3. Graph plotting the relationship between the mass of UV-curing resin in the sample and its bending stress.

V. Prototype Robot

A. Structure Fabrication

In this section, we describe the method used to fabricate the prototype robot. Fig. 4(a) shows the appearance of the prototype robot. In this case, a urethane foam sponge is cut out a 2 cm × 7 cm×3 cm rectangle. The density of the urethane foam sponge was 22 kg/m^3. We then soaked one side of the 2 cm × 7 cm surface of the sponge in the UV-curing resin for a few millimeters. After the UV-curing resin fully penetrated the target surface, the sponge was placed on a polyethylene sheet with the soaked surface down. The sponge was moved to the polyethylene sheet to make it easier for the sponge to separate from the ground surface after curing. Then, the sponge on the polyethylene sheet was placed under a UV light and irradiated from the top. After the sponge was cured for a sufficient period, it was removed and turned upside down, and UV light was applied again to complete the curing process. The basic structure of the robot primarily comprised coarse urethane foam sponge and UV-curing resin.

B. Power Source Installation and Drive Mechanism

Here, we discuss the implementation of the robot's power supply and how the robot moves. The locomotion of the robot was achieved using a DC vibration motor. The DC vibration motor had an eccentric weight attached to its rotating part to generate vibration synchronized with motor rotation. This was glued to the top front of the sponge, which was previously hardened via UV-curing resin, with the hardened side of the sponge on the top side.

In addition, as shown in Fig. 4(b), a climbing skin with a ratchet structure was attached to the nonhardened 2 cm × 7 cm side (the bottom of the sponge). This implementation provides low friction when moving forward. Fig. 4(c) shows a schematic diagram of the prototype robot.

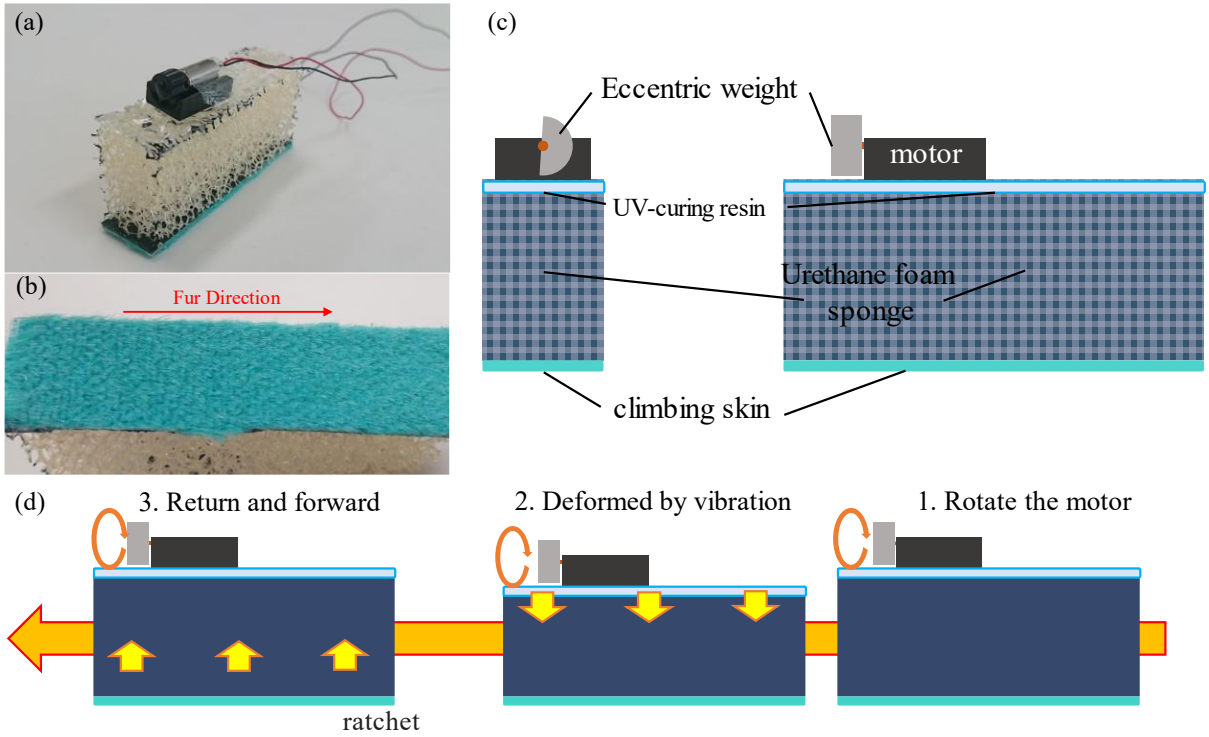

Fig. 4. Driving mechanism of the proposed robot using vibration motors. (a) Appearance of the prototype robot. (b) Ratchet structure of the climbing skin attached to the bottom of the robot. (c) Schematic diagram of the components of the proposed robot. (d) Conceptual diagram of the forward movement mechanism by vibration propulsion.

The robot's driving mechanism is described as follows. The mechanism is generally referred to as vibration propulsion [25]. Fig. 4(d) shows a schematic diagram of the series of driving mechanisms. First, a current is applied to the vibration motor to rotate the eccentric weight. The generated vibrations are transmitted to the entire robot. During this process, the force that distorts the sponge is applied to the middle layer of the sponge. The distorted sponge then returns to its original shape due to its elasticity. As a result, the frictional forces of the climbing skin create a sliding force on the surface. The direction of the generated force is fixed due to the ratchet structure of the climbing skin. Thus, the robot can move forward by repeating these movements at the period of oscillation.

VI. Experimental Demonstration and Results

Finally, we demonstrate the operation of the proposed robot. In this section, we discuss a robot with the shape shown in Fig. 5(a), which is a parallel connection of the fabricated robots discussed in the previous sections. We expected that this configuration would make it possible to change direction by driving either the left or right vibration motor. The size of the basic structural part of this robot was approximately 8 cm in length and width, and 3 cm in thickness, with the front center portion cut out to roughly 4 cm × 6 cm × 3 cm. The method used to manufacture this robot was essentially the same as that described in the Section V.

With this robot, we initially measured the moving speed. This experiment was conducted on a desk with a melamine resin decorative board top. The left and right motors were connected to their own batteries. Fig. 5(b) shows an example of the experiment. The distance traveled was approximately 40 cm in a straight line. We measured the time required to travel this distance four times and calculated the average value. As a result, the average moving speed of this robot was 0.93 cm/s.

In addition, we conducted an experiment assuming that the robot shown in Fig. 5(a) was equipped with a power supply. Here, a battery (mass: 11 g) was fixed to the upper rear of the robot, and the speed of the robot's movement was measured. Fig. 5(c) shows an example of this experiment. Under this condition, we found that the average moving speed of the robot was 0.56 cm/s.

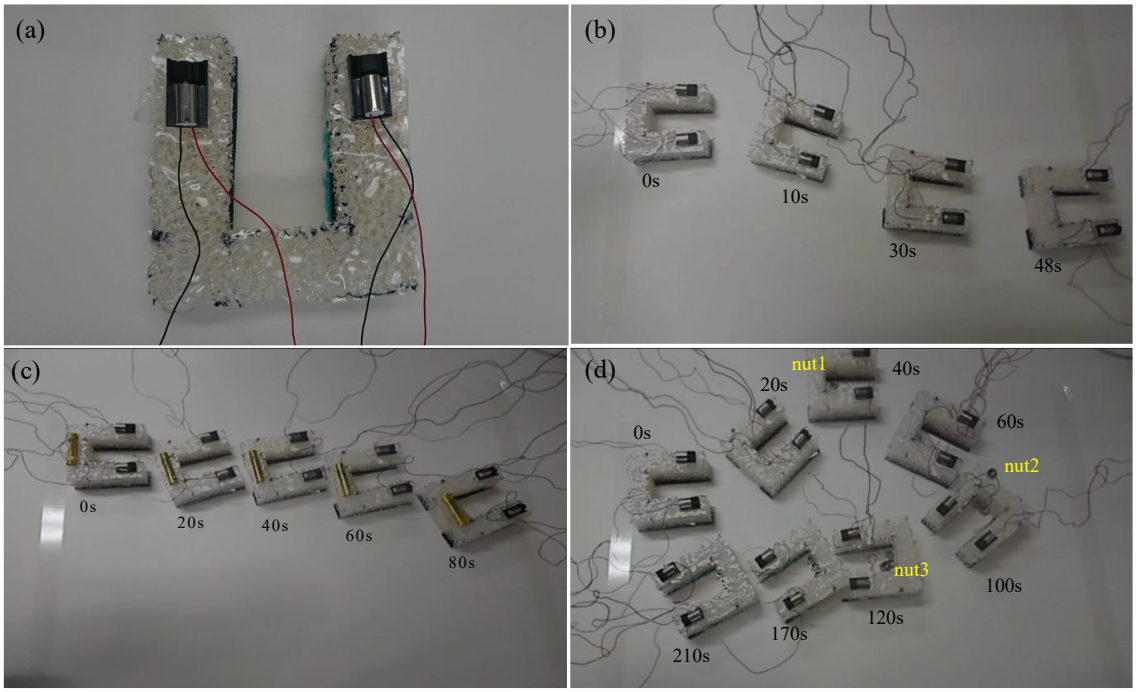

Fig. 5. Demonstration of the robot's drive. (a) Appearance of the demonstration robot. (b) View of the robot moving in a straight line. (c) View of the robot moving in a straight line with a weight on it. (d) View of the collection and transport of nuts by the robot. The elapsed time up to that point is shown near each robot. The initial position of the nut is also shown in (d).

Finally, we conducted an experiment that assumed the collection and transport of objects. Here, we used three common hexagonal nuts weighing approximately 2 g as collection objects. These objects were placed at three locations on the same tabletop as the robot. The objects were contained in turn in the empty space in the center of the robot and transported in a dragging manner. This experiment is shown in Fig. 5(d). We found that the robot could collect and transport all three hex nuts. However, the robot's movement speed decreased with each collected hex nut. In particular, the robot's movement speed decreased significantly after the third hex nut was recovered and was two to three times slower than when nothing was being carried.

VII. Discussion and Conclusion

We have proposed the conceptual design and a prototype for a robot that can be stored in a small and soft state and then become large and rigid when used. To clarify our concept, we developed the robot that enabled saving space during transportation by vacuum compressing the robot, which was possible due the inherent elasticity of the robot's constituent materials. The basic component of this robot can be reduced to 15% of its original volume during transportation. After transportation, it can be restored to its original shape and size by releasing it from compression. In addition, the robot gains rigidity by adding UV-curing resin to its sponge structure and exposing it to sunlight in a natural environment, which allows it to be used as a disaster response robot. We confirmed that the proposed robot can execute basic forward vibration propulsion using a vibration motor as a driving source.

In addition, a three-point bending test was conducted to investigate the mechanical strength of the robot's basic structure. A compression test was also conducted, and the sample used in the test was 3 cm × 3 cm×2 cm and contained approximately 3 g of UV-cured resin. The compression test was terminated when the measurement limit of 500 N was reached, at which time the sample was compressed by approximately 3 mm. This and the three-point bending test results indicate that the urethane foam sponge cured by UV-curing resin is sufficiently strong against compression. In addition, we confirmed that the proposed robot exhibits sufficient rigidity after curing.

In addition, in this three-point bending test, variations in bending stress were observed when the mass of the UV-cured resin was relatively large. This is thought to be due to the lack of uniformity in the composition of the samples. In this study, we manually penetrated and cured the UV-cured resin into the sponge. This may have caused a slight bias in the UV resin in the sponge. We believe that this bias caused bending to occur in areas where the density of the UV-curing resin was smaller.

In this study, we soaked a few millimeters of the top surface of the robot in UV-curing resin and cured it. This was performed because we found that when robot that was completely soaked with resin and cured, it had a lower forward speed than the partially soaked robot. We consider that this was due to the movement method, i.e., the vibration motor. When a urethane foam sponge was cured with UV curing resin, its rigidity increases; however, its elasticity characteristic is lost. The loss of elasticity has a negative effect on the robot's movement. In addition, there was a significant reduction in movement speed during the object collection and transport demonstration. We believe that resistance of the objects being collected affected the

vibrational propulsion of the robot. Therefore, in the future, we plan to conduct a more detailed mechanical investigation of the impact of movement by vibration motors on the robot. In addition, we will consider other propulsion mechanisms to create more practical robots.

CONFLICT OF INTEREST

The authors declare no conflict of interest.

AUTHOR CONTRIBUTIONS

K.O. contributes the conceptualization, methodology, validation, investigation, and original draft preparation. M. M. contributes the conceptualization, supervision, project administration, and review and editing. All authors had approved the final version.

FUNDING

This research was supported by JSPS KAKENHI Grant Number JP20H02412 and JP23K17770.

REFERENCES

[1] X. Zhang, Y. An, G. Fu *et al.*, "Survey on key technology of Robocup rescue robot," in *Proc. The 38th Chinese Control Conference*, 2019, pp. 4746–4750.
[2] T. Tsumaki, H. Kato, and E. F. Fukushima, "Multi crawler robot—The development of the 4 crawler moving mechanism and the extended development of the coupled robot," *Journal of the Robotics Society of Japan*, vol. 36, no. 8, pp. 551–558, 2018.
[3] M. Sutoh and K. Shimizu, "Super-fiber tracked robot VAMOS (Development and experimental evaluation of super-fiber track)," *Transactions of the JSME*, vol. 85, no. 878, 2019.
[4] K. Nagatani, S. Kiribayashi, Y. Okada *et al.*, "Emergency Response to the nuclear accident at the Fukushima Daiichi nuclear power plants using mobile rescue robots," *Journal of Field Robotics*, vol. 30, no. 1, pp. 44–63, 2013.
[5] T. Furuta, T. Yoshida, T. Nishimura *et al.*, "Development of the exploring robot toward future indoor surveillance missions in the Fukushima Daiichi nuclear," *Journal of the Robotics Society of Japan*, vol. 32, no. 2, pp. 92–97, 2014.
[6] P. Hebert, M. Bajracharya, J. Ma *et al.*, "Mobile manipulation and mobility as manipulation—Design and algorithms of RoboSimian," *Journal of Field Robotics*, vol. 32, no. 2, pp. 255–274, 2015.
[7] K. Kamikawa, T. Arai, Y. Mae *et al.*, "Expansion of movable area of multi legged robot by rotational gait," *Journal of the Robotics Society of Japan*, vol. 28, no. 2, pp. 231–240, 2010.
[8] A. Saito, K. Nagayama, Y. Homma *et al.*, "Multi-legged robot for 3-dimensional environments—Adaptive mechanism using Flexible body and legs," *SICE Journal of Control, Measurement, and System Integration*, vol. 54, no. 9, pp. 695–704, 2018.
[9] M. Mori, H. Yamada, and S. Hirose, "Design and development of active cord mechanism 'ACM-R3' and its 3-dimensional locomotion control," *Journal of the Robotics Society of Japan*, vol. 23, no. 7, pp. 886–897, 2005.
[10] S. Satomura, M. Hara, H. Fukushima *et al.*, "Control of a snake-like robot using the screw drive mechanism," *Journal of the Robotics Society of Japan*, vol. 25, no. 5, pp. 779–784, 2007.
[11] M. Inazawa, T. Takemori, M. Tanaka *et al.*, "Motion design for a snake robot negotiating complicated pipe structures of a constant diameter," in *Proc. 2020 IEEE International Conference on Robotics and Automation*, 2020, pp. 8073–8079.
[12] T. Kamegawa, T. Akiyama, S. Sakai *et al.*, "Development of a separable search-and-rescue robot composed of a mobile robot and a snake robot," *Advanced Robotics*, vol. 34, no. 2, 2020.
[13] R. Y. Hutama, M. M. Khalil, and T. Mashimo, "A millimeter-scale rolling microrobot driven by a micro-geared ultrasonic motor," *IEEE Robotics and Automation Letters*, vol. 6, no. 4, pp. 8158–8164, 2021.
[14] E. T. K. Chiang, T. Urakubo, and T. Mashimo, "Lift generation by a miniature piezoelectric ultrasonic motor-driven rotary-wing for Pico air vehicles," *IEEE Access*, vol. 10, pp. 13210–13218, 2022.
[15] U. Scarfogliero, C. Stefanini, and P. Dario, "A bioinspired concept for high efficiency locomotion in micro robots: The jumping robot," in *Proc. IEEE International Conference on Robotics and Automation*, 2006, pp. 4037–4042.
[16] C. Hu, F. Arvin, C. Xiong *et al.*, "Bio-inspired embedded vision system for autonomous micro-robots: The LGMD case," *IEEE Transactions on Cognitive and Developmental Systems*, vol. 9, no. 3, pp. 241–254, 2017.
[17] X. Yang, R. Tan, H. Lu *et al.*, "Starfish Inspired milli soft robot with omnidirectional adaptive locomotion ability," *IEEE Robotics and Automation Letters*, vol. 6, no. 2, pp. 3325–3332, 2021.
[18] R. Qi, T. L. Lam, and Y. Xu, "Mechanical design and Implementation of a soft inflatable robot arm for safe human-robot interaction," in *Proc. IEEE International Conference on Robotics & Automation*, 2014, pp. 3490–3495.
[19] R. Niiyama, M. Ikeda, and Y. A. Seong, "Inflatable humanoid cybernetic avatar for physical human–robot interaction," *International Journal of Automation Technology*, vol. 17, no. 3, pp. 277–283, 2023.
[20] S. Voisembert, A. Riwan, N. Mechbal *et al.*, "A novel inflatable robot with constant and continuous volume," *IEEE International Conference on Robotics and Automation*, 2011, pp. 5843–5848.
[21] H.-J. Kim, Y. Tanaka, A. Kawamura *et al.*, "Development of an inflatable robotic arm system controlled by a Joystick," in *Proc. 24th IEEE International Symposium on Robot and Human Interactive Communication*, 2015, pp. 664–669.
[22] R. Tatara, N. Nomaguchi, A. Kawamura *et al.*, "Development of an inflatable robotic arm on mobile platform for fetch-and-give tasks," in *Proc. IEEE/SICE International Symposium on System Integration*, 2019, pp. 707–711.
[23] R. Niiyama, D. Rus, and S. Kim, "Pouch motors: Printable/inflatable soft actuators for robotics," in *Proc. IEEE International Conference on Robotics and Automation*, pp. 6332–6337, 2014.
[24] S. Chung, A. Coutinho, and H. Rodrigue, "Manufacturing and Design of Inflatable Kirigami Actuators," *IEEE Robotics and Automation Letters*, vol. 8, no. 1, pp. 25–32, 2023.
[25] K. Ioi, "Study on mobile micro-robot using centrifugal force," *JRSJ*, vol. 17, no. 3, pp. 396–401, 1999.